High-order above-threshold ionization from a coherent superposition of states

Dejan B. Milošević [●],[1,2] Benjamin Fetić [●],[1] and Predrag Ranitovic[3,4]

[1]*University of Sarajevo, Faculty of Science, Zmaja od Bosne 35, 71000 Sarajevo, Bosnia and Herzegovina*
[2]*Academy of Sciences and Arts of Bosnia and Herzegovina, Bistrik 7, 71000 Sarajevo, Bosnia and Herzegovina*
[3]*Faculty of Physics, University of Belgrade, Studentski Trg 12, 11001 Belgrade, Serbia*
[4]*Chemical Sciences Division, Lawrence Berkeley National Laboratory, Berkeley, California 94720, USA*

Quantum theory of high-order above-threshold ionization (HATI) of atoms, prepared in a coherent superposition of bound states, by a strong laser field is formulated. Numerical results are obtained using the solutions of the time-dependent Schrödinger equation and the improved strong-field approximation. As an example, coherent superposition of the excited $2s$ and $2p$ states of the He atom is used. Applying a two-level model, it is shown how the relative amplitude and phase of the states in this coherent superposition can be controlled with a weak resonant laser pulse. Numerical results presented for HATI by a strong nonresonant probe laser pulse confirm that the photoelectron spectra and the momentum distributions strongly depend on the relative phase of the states in the prepared coherent superposition. For the case of HATI by a strong resonant laser pulse, we modify our strong-field-approximation theory by applying the two-level model to describe the time evolution of the atomic bound state before the instant of ionization. Contrary to the HATI from a single state by a long laser pulse, the corresponding photoelectron spectra of HATI from the coherent superposition of states depend on the carrier-envelope phase of the resonant ionizing pulse. Therefore, the strong-field ionization from a coherent superposition of states by a resonant laser pulse can be used to determine the carrier-envelope phase for long pulses for which the standard methods such as stereo–above-threshold ionization technique fail. The results strongly depend on the relative amplitude and phase of states in the coherent superposition of states, which can be controlled with a weak resonant laser pulse.

I. INTRODUCTION

The main subject of strong-field physics is the study of strong-laser-field-induced atomic and molecular processes [1]. These processes enable insights into the dynamics of electrons in atoms and molecules on the subfemtosecond timescale, which stimulated the development of attoscience [2,3]. Theoretical analysis of these processes is usually based on the strong-field approximation (SFA) in which the electron is initially bound in the atomic or molecular ground state and in intermediate and final states is driven by the laser field alone (in the so-called Volkov state). Excited states are usually neglected. However, it is desirable to obtain information about the atomic or molecular level structure and, more importantly, about the electron dynamics in a bound potential. Such information can be obtained from the spectra of high-order harmonic photons [in high-order harmonic generation (HHG) [4–8]] and photoelectron spectra (in (high-order) above-threshold ionization [(H)ATI] [9–12] as well as nonsequential multiple ionization [13,14]). For this purpose it is necessary to prepare an atomic or molecular initial state in a superposition of bound states. This can be achieved by exciting atoms or molecules using HHG radiation with harmonic photon energy resonant with the transition from the ground to an excited state [15–20] or using a free-electron laser [21].

First observation of HHG from an optically prepared excited state of a rubidium atom irradiated simultaneously by an intense 3.5-μm fundamental field and a weak cw diode laser was reported in [22]. An orders-of-magnitude increase in harmonic yield was observed when the excited states were populated. Theoretically, HHG from a coherent superposition of ground and excited atomic states was considered in [23–28]. An increase in HHG efficiency in comparison to HHG from the ground state alone was observed. In [29] the mapping of the attosecond electron wave-packet motion was demonstrated using a two-state one-dimensional molecular model.

In addition to HHG from atomic and molecular gases, HHG was observed in experiments with different media such as ablation plasma. A strong resonance enhancement of single harmonics was observed in ablation plasma of metals [30] (for more information see the review articles [31,32] and monograph [33]). The positive ions of such ablation plasma have a large absorption strength for the transition between the ground state and a metastable excited state which is embedded in the continuum. The theory of HHG from a coherent superposition of states [27], adjusted to this case of metastable excited states, was used to qualitatively explain experimental results [34–36]. A related explanation is based on autoionizing states and the four-step model [37].

The SFA neglects the role of excited states in the ionization process. However, it is well known that excited states can play a role in strong-field processes. We mention Freeman resonances [38], the work [39] in which it was shown (by

013109-1

probing with a second laser) that the atoms subjected to an intense subpicosecond laser pulse survive in excited states, observation that neutral and ionic Rydberg states of Kr and Xe are populated during the interaction of ground-state atoms with intense 100-fs 770-nm laser pulses [40], recollision excitation with subsequent ionization [41], multiphoton excitation spectroscopy [42], resonance-enhanced multiphoton ionization [43], and frustrated tunneling ionization (FTI) [44]. If the dressing laser field couples bound states to the continuum, light-induced structures may appear [45,46]. A method of measurement of Stark shift in excited helium was considered in [47,48]. We should also mention observation of an exceptional stability of Rydberg atoms in strong laser fields [49] (for strong-field stabilization with much more intense pulses, see the review article [50]). Strong-field ionization from a coherent superposition of electronic states of Ar^+ ion was studied in [51]. More precisely, a pump-probe scheme is used and a spin-orbit wave packet is launched via the first ionization of the neutral Ar atom and then the wave packet of Ar^+ is probed as a function of time by the second pulse that produces an Ar^{2+} ion. As a result, information about electron momentum distributions and the tunneling process itself is obtained. The authors of Ref. [51] were also studying creation and survival of autoionizing states in krypton and argon by strong laser fields over a large range of wavelengths [52]. For more recent experimental results we mention Refs. [53–55]. In [53] intense optical attosecond pulses are synthesized which allows generation of electronic bound-state wave packets in atoms involving electronic intershell coherences without strong coupling to ionization channels. Strong-field excitation in Ne and Ar in both the tunneling and multiphoton regimes was considered in [54] and an enhancement of the excitation of Rydberg states in the vicinity of a channel closing was observed. In [55] HHG from He atoms excited by intense few-cycle laser pulses via FTI was considered. For more references on the excitation and probing of electronic coherences in atoms and a theoretical formulation in terms of the time evolution of the (reduced) density matrix and the Liouville operator formulation, see the recent paper [56]. It should be mentioned that, very recently, strong-field ionization of He prepared in an excited p state was considered in [57].

A coherent superposition of atomic states can be created using a weak resonant laser field with photon energy equal to the energy difference between the states which form this superposition. In Sec. II we show how the relative amplitude and phase of the states forming this superposition can be controlled with the parameters of this resonant laser pulse. We first prove this using a two-level model and then confirm this model using exact solutions of the three-dimensional (3D) time-dependent Schrödinger equation (TDSE) in Sec. III. In Sec. IV we present the improved SFA (ISFA) theory of HATI from a coherent superposition of states for the case when the laser field is nonresonant. Our numerical results show that the photoelectron spectra and momentum distributions strongly depend on the values of the relative phase between the states in the superposition used. In Sec. V we consider the possibility that the wavelength of the ionizing strong laser pulse is resonant with the transition between the atomic states in the superposition used. For this case we present the corresponding ISFA and TDSE numerical results. Ionization from a coherent

superposition of states allows for different paths of the ionization process. We show how the interplay between different interference paths manifests in the photoelectron momentum distribution. A discussion and our conclusions are given in Sec. VI. We also provide Appendix A, in which we present analytical results for the dipole matrix elements that appear in the SFA, and Appendix B, in which we estimate the optimal parameters for observation of new effects in HATI from a coherent superposition of states. We use atomic system of units ($e = \hbar = m_e = 1$).

II. TWO-LEVEL SYSTEM IN A LASER FIELD

Consider a two-level system with the Hamiltonian H_0, having the eigenstates $|\psi_j\rangle$ and the eigenenergies E_j, $j = 1, 2$. The most general wave function of this system is [58]

$$|\Psi(t)\rangle = \sum_{j=1,2} c_j(t)|\psi_j\rangle e^{-iE_jt}, \quad c_j(t) = a_j(t)e^{i\varphi_j(t)}, \quad (1)$$

where $a_j(t)$ and $\varphi_j(t)$ are real and

$$H_0|\psi_j\rangle = E_j|\psi_j\rangle, \quad \langle\psi_k|\psi_j\rangle = \delta_{kj}, \quad \sum_j a_j^2(t) = 1. \quad (2)$$

We introduce the interaction with a linearly polarized laser field $E(t)$ having the amplitude E_0, angular frequency ω, envelope $f(t)$, and carrier-envelope phase φ_R:

$$E(t) = E_0 f(t) \cos(\omega t + \varphi_R). \quad (3)$$

The envelope can, for example, be sine squared with the total pulse duration equal to an integer number n_p of optical cycles $T = 2\pi/\omega$,

$$f(t) = \sin^2\left(\frac{\omega t}{2n_p}\right), \quad t \in [0, T_p], \quad T_p = n_pT. \quad (4)$$

The intensity of this field is $I = E_0^2$ and the pulse duration, defined as the full width at half maximum of the intensity, is $\tau_p = 0.364\,06T_p$ [59].

The wave function $|\Psi(t)\rangle$ satisfies the time-dependent Schrödinger equation

$$i\frac{\partial|\Psi(t)\rangle}{\partial t} = H(t)|\Psi(t)\rangle, \quad H(t) = H_0 + zE(t), \quad (5)$$

where $H(t)$ is the total Hamiltonian of our two-level system in interaction with the laser field in the dipole approximation and length gauge and we suppose that the laser field is polarized along the quantization axis z so that $\mathbf{r} \cdot \mathbf{E}(t) = zE(t)$. Introducing (1) into (5), we obtain the system of differential equations for the coefficients $c_j(t)$,

$$\dot{c}_1(t) = -i\mu f(t)[e^{i\Delta\omega t + i\varphi_R} + e^{-i(\omega+\omega_0)t - i\varphi_R}]c_2(t),$$
$$\dot{c}_2(t) = -i\mu^* f(t)[e^{-i\Delta\omega t - i\varphi_R} + e^{i(\omega+\omega_0)t + i\varphi_R}]c_1(t), \quad (6)$$

where we use the relation $\langle\psi_j|z|\psi_j\rangle = 0$ and introduce the notation

$$\mu = E_0\langle\psi_1|z|\psi_2\rangle/2, \quad \omega_0 = E_2 - E_1, \quad \Delta\omega = \omega - \omega_0. \quad (7)$$

Supposing that the detuning $\Delta\omega$ is such that $|\Delta\omega| \ll \omega_0$, we apply the rotating-wave approximation [58], according to which $e^{\pm i\Delta\omega t}$ is slowly varying while $e^{\pm i(\omega+\omega_0)t}$ is rapidly

varying and therefore when integrated gives approximately zero. Neglecting the corresponding terms in Eq. (6), we obtain the system

$$\dot{c}_1(t) = -i\mu f(t)e^{i(\Delta\omega t + \varphi_R)}c_2(t),$$
$$\dot{c}_2(t) = -i\mu^* f(t)e^{-i(\Delta\omega t + \varphi_R)}c_1(t). \quad (8)$$

The solution of this system in the resonant case ($\Delta\omega = 0$) and for μ real is

$$c_1(t) = c_1(0)\cos[F(t)] - ic_2(0)\sin[F(t)]e^{i\varphi_R},$$
$$c_2(t) = c_2(0)\cos[F(t)] - ic_1(0)\sin[F(t)]e^{-i\varphi_R}, \quad (9)$$

where for the envelope (4) we have

$$F(t) = \mu \int_0^t f(t')dt' = \frac{n_p\mu}{2\omega}\left[\frac{\omega t}{n_p} - \sin\left(\frac{\omega t}{n_p}\right)\right]. \quad (10)$$

For the initial condition $c_2(0) = 1$ and $c_1(0) = 0$, we obtain

$$c_1(t) = -i\sin[F(t)]e^{i\varphi_R}, \quad c_2(t) = \cos[F(t)]. \quad (11)$$

For example, for the hydrogenic $2s$ and $2p$ states we have

$$\langle\psi_{2s}|z|\psi_{2p}\rangle = -3, \quad \mu = \mu^* = -\frac{3E_0}{2}. \quad (12)$$

The ionization potentials of the excited states of He atoms are (see Appendix B)

$$I_p(2s) = -E_1 = 3.972 \text{ eV}, \quad I_p(2p) = -E_2 = 3.369 \text{ eV}, \quad (13)$$

so $\lambda_0 = 2057$ nm where $\omega_0 = 2\pi c/\lambda_0$. Using a free-electron-laser or high-order-harmonic source of photons, we excite the ground $1s$ state of He to the $2p$ state [according to selection rules, this excitation is possible; we do not calculate the probability of the transition $1s \to 2p$, but we suppose that some of the atoms (not 100%) in He gas are excited to the $2p$ state, which is the initial state for our calculations]. Then we expose the He gas in this $2p$ excited state to a resonant IR laser having wavelength λ_0. Therefore, the initial condition is $c_2(0) = c_{2p}(0) = 1$ and $c_1(0) = c_{2s}(0) = 0$ and the result (11) with (10) and (12) is valid. At the end of the laser pulse we have $F(n_pT) = -F_p$, $F_p = 3n_pA_0\pi/2$, and $A_0 = E_0/\omega$. The population is completely transferred from the $2p$ state to the $2s$ state if

$$3n_pA_0 = 2j + 1, \quad j = 0, 1, 2, \ldots. \quad (14)$$

In Fig. 1, for a fixed wavelength of 2057 nm, we present the parameter $3n_pA_0$ as a function of the laser intensity for pulse duration from one to ten optical cycles. If $3n_pA_0$ is even (odd), the population of the $2s$ state is zero (one). The horizontal line in Fig. 1 intersects the curves $3n_pA_0$ for particular values of the intensity. For example, for $n_p = 4$ (red circles) and for an intensity of 1.2×10^{11} W/cm^2 we have $3n_pA_0 \approx 1$, so the population is completely transferred from the $2p$ to the $2s$ state.

After the IR pulse is gone ($t \geqslant T_p$), the excited He state is the superposition

$$|\Psi(t)\rangle = \big[\sin(F_p)e^{i(\varphi_R - \pi/2)}|\psi_{2s}\rangle e^{-iE_{2s}t}$$
$$+ \cos(F_p)|\psi_{2p}\rangle e^{-iE_{2p}t}\big]. \quad (15)$$

The relative amplitude for the $2s$ and $2p$ states is $\tan(F_p)$ and depends on the pulse duration n_p and the field amplitude E_0.
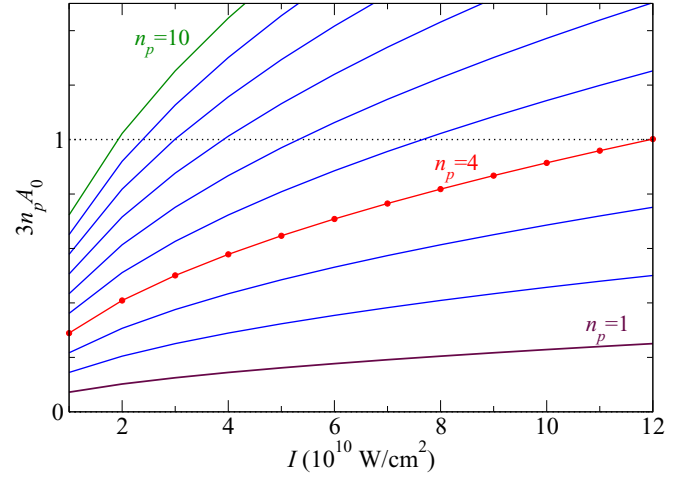

FIG. 1. Parameter $3n_pA_0$ as a function of the laser intensity in units of 10^{10} W/cm^2 for different pulse durations (n_p is from 1 to 10). The laser pulse is sine squared with a total duration of n_p optical cycles and a wavelength of 2057 nm.

On the other hand, the relative phase between the $2s$ and $2p$ states is $\varphi_R - \pi/2$ and depends on the carrier-envelope phase of the few-cycle IR pulse. For example, for $n_p = 4$ and the intensity $I = E_0^2 = 6.88 \times 10^{10}$ W/cm^2 we obtain $a_{2p} = \cos(F_p) = 0.37$. We will use this ratio in our calculations of the HATI spectra.

III. NUMERICAL SOLUTION OF THE TIME-DEPENDENT SCHRÖDINGER EQUATION

Our numerical method for solving the 3D TDSE within the single-active-electron approximation and dipole approximation is described in detail in [60]. This method is here applied to a coherent superposition of states. We first solve the stationary Schrödinger equation in order to obtain the wave functions and energies of the $2s$ and $2p$ excited states of the He atom. We model the single-active-electron potential using the spherically symmetric potential

$$V(r) = -\frac{1 + a_1e^{-a_2r} + a_3re^{-a_4r} + a_5e^{-a_6r}}{r}, \quad (16)$$

where the parameters a_j are chosen such that they give correct values for the energies of the chosen atomic state. For the excited $2s$ and $2p$ states of the He atom these parameters are $a_1 = 2.201$, $a_2 = 5.6606$, $a_3 = -4.054$, $a_4 = 2.740$, $a_5 = 0.5810$, and $a_6 = 1.4623$. Using the potential (16), we calculated the ionization potential of the $2s$ and $2p$ states and obtained $I_p(2s) = 3.972$ eV and $I_p(2p) = 3.369$ eV.

After obtaining the wave function which is a coherent superposition of the excited states by solving the stationary Schrödinger equation, we propagate this wave function under the influence of the laser field by numerically solving the TDSE

$$i\frac{\partial\Psi(\mathbf{r}, t)}{\partial t} = [H_0 + V_I(t)]\Psi(\mathbf{r}, t), \quad (17)$$

where $H_0 = -\nabla^2/2 + V(r)$ is the field-free Hamiltonian and $V_I(t)$ is the interaction operator in the dipole approximation and length gauge [$V_I(t) = zE(t)$] or velocity gauge
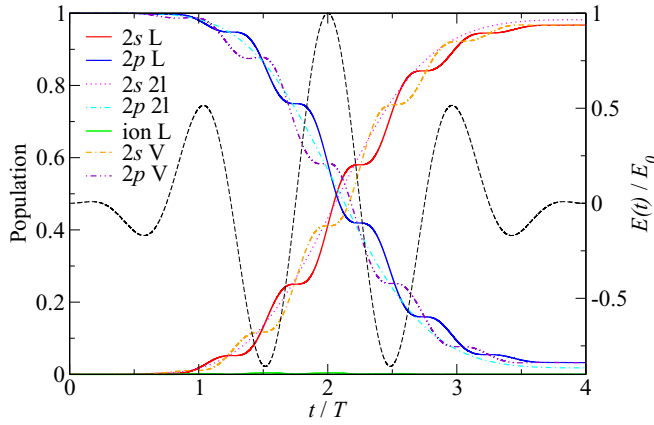
FIG. 2. Survival probabilities of the $2s$ (red solid line for the length gauge L and orange dot-dashed line for the velocity gauge V, labeled $2s$] and $2p$ (blue solid line for length gauge and violet double-dot–dashed line for velocity gauge, labeled $2p$) states and the ionization probability (green line labeled ion L), obtained using the TDSE solutions, presented as functions of the time in optical periods. Populations of the $2s$ (magenta dotted line) and $2p$ (cyan dot-dashed line) states, according to the two-level model (labeled 2l) are also presented. The linearly polarized laser electric-field vector is presented on the right-hand ordinate by a black dashed line. The laser pulse is sine squared with a total duration of four cycles, carrier-envelope phase $\varphi_R = 0$, wavelength of 2057 nm, and intensity of 1×10^{11} W/cm^2.

$[V_I(t) = -iA(t)\partial_z]$ (in all calculations, except in Fig. 2, we use the velocity gauge since the calculations are faster in this gauge). At the end of the laser-atom interaction at the time $t = T_p$ we obtain the final time-dependent wave function $\Psi(\mathbf{r}, T_p)$ from which we extract the corresponding photoelectron momentum distribution $P(E_\mathbf{p}, \theta)$ by projecting $\Psi(\mathbf{r}, T_p)$ onto the continuum states $\Phi_\mathbf{p}^{(-)}(\mathbf{r})$ of the field-free Hamiltonian,

$$P(E_\mathbf{p}, \theta) = 2\pi p |\langle \Phi_\mathbf{p}^{(-)} | \Psi(T_p) \rangle|^2, \quad (18)$$

where $\mathbf{p} = (p_z, p_x) = (p\cos\theta, p\sin\theta)$. The continuum states $\Phi_\mathbf{p}^{(-)}$ have to obey the incoming boundary condition and we calculate them by solving the radial Schrödinger equation for the fixed photoelectron kinetic energy $E_\mathbf{p} = \mathbf{p}^2/2$. We also calculate survival probabilities of the $2s$ and $2p$ states as functions of time using the formula

$$|c_j(t)|^2 = |\langle \psi_j | \Psi(t) \rangle|^2, \quad j = 2s, 2p. \quad (19)$$

It should be mentioned that only the probabilities at the end of the laser pulse, $c_j(T_p)$, are observable, while the quantities $c_j(t)$ are gauge dependent (in principle, they can be defined in a gauge-covariant way, but this goes beyond the consideration of the present paper [61,62]).

As we have mentioned, we will present numerical results for the excited $2s$ and $2p$ states of the helium atom. Using a free-electron-laser or a high-order-harmonic source of photons, we excite the ground $1s$ state of He to the $2p$ state. Then we act with the resonant laser having the wavelength $\lambda_0 = 2057$ nm on this $2p$ state. The final state at the end of the laser pulse is a superposition of the $2s$, $2p$, and continuum states. Initially, at $t = 0$, only the $2p$ state is occupied,

i.e., $c_{2p}(0) = 1$ and $|\Psi(0)\rangle = |\psi_{2p}\rangle$. In Fig. 2 we compare populations obtained using the two-level model and survival probabilities obtained using the TDSE solutions as functions of the time, for $n_p = 4$ and an intensity of 1×10^{11} W/cm^2. We see that, in accordance with the results of Fig. 1, the population is largely transferred from the $2p$ state to the $2s$ state. The TDSE results, in both length and velocity gauges, and the two-level-model results agree very well. The reason is that for the low intensity used the ionization probability is low (see the green line labeled "ion L" in Fig. 2; this result is obtained in the length gauge).

IV. IMPROVED STRONG-FIELD APPROXIMATION FOR IONIZATION BY A NONRESONANT LASER PULSE

The differential ionization probability $W_\mathbf{p}$ for the emission of an electron with the energy $E_\mathbf{p}$ into the solid-angle element $d\Omega_{\hat{\mathbf{p}}}$ is [59]

$$W_\mathbf{p} = \frac{|M_{fi}|^2 d\mathbf{p}}{dE_\mathbf{p} d\Omega_{\hat{\mathbf{p}}}} = p|M_{fi}|^2. \quad (20)$$

Within the ISFA, the ATI transition amplitude is $M_{fi} = M_{fi}^{\text{dir}} + M_{fi}^{\text{res}}$, where the direct and rescattering matrix elements are

$$M_{fi}^{\text{dir}} = -i \int_0^{T_p} dt_0 e^{iS_\mathbf{p}(t_0)} \langle \mathbf{p} + \mathbf{A}(t_0) | \mathbf{r} \cdot \mathbf{E}(t_0) | \psi_i(t_0) \rangle, \quad (21)$$

$$M_{fi}^{\text{res}} = (-i)^2 \int_0^{T_p} dt \int_0^t d\tau \left(\frac{2\pi}{i\tau}\right)^{3/2} e^{iS_\mathbf{p}(t)} \langle \mathbf{p} | V | \mathbf{q} \rangle$$
$$\times e^{i[S_\mathbf{q}(t_0) - S_\mathbf{q}(t)]} \langle \mathbf{q} + \mathbf{A}(t_0) | \mathbf{r} \cdot \mathbf{E}(t_0) | \psi_i(t_0) \rangle. \quad (22)$$

Here $t_0 = t - \tau$, $\mathbf{E}(t) = -d\mathbf{A}(t)/dt$ is the electric-field vector, $dS_\mathbf{p}(t)/dt = [\mathbf{p} + \mathbf{A}(t)]^2/2$, $\mathbf{p}$ is the final electron momentum at the detector, $|\mathbf{p}\rangle$ is a plane-wave ket vector such that $\langle \mathbf{r} | \mathbf{p} \rangle = (2\pi)^{-3/2} \exp(i\mathbf{p} \cdot \mathbf{r})$, $V(\mathbf{r})$ is the rescattering potential, $\mathbf{q} = -[\boldsymbol{\alpha}(t) - \boldsymbol{\alpha}(t_0)]/\tau$ is the electron stationary momentum, and $\boldsymbol{\alpha}(t) = \int^t \mathbf{A}(t')dt'$. The initial atomic bound state is a linear superposition of the orthonormal states $|\psi_j\rangle$ with the energies E_j and the coefficients $c_j(t_0)$:

$$|\psi_i(t_0)\rangle = \sum_j c_j(t_0) |\psi_j\rangle e^{-iE_j t_0}. \quad (23)$$

The direct transition amplitude corresponds to the process in which the electron, liberated from the atom at the time t_0 via the interaction $\mathbf{r} \cdot \mathbf{E}(t_0)$, goes directly to the detector with the asymptotic momentum $\mathbf{p}$. The rescattering transition amplitude is described by the so-called three-step model: The electron, liberated (virtually) at the time t_0, propagates in the laser field during the travel time τ up to the time $t = t_0 + \tau$, when it returns to the parent ion and elastically scatters off the potential $V(\mathbf{r})$, and then moves towards the detector reaching it with the asymptotic momentum $\mathbf{p}$. The rescattering potential is modeled by Eq. (16) with the Coulomb potential screened with the factor $\exp(-0.3r)$.

The photoelectron energy spectra and momentum distributions in strong-field ionization from the ground atomic state are explored in detail (see, for example, the review articles [12,59] and references therein). For electron emission in the laser-field polarization direction the low-energy
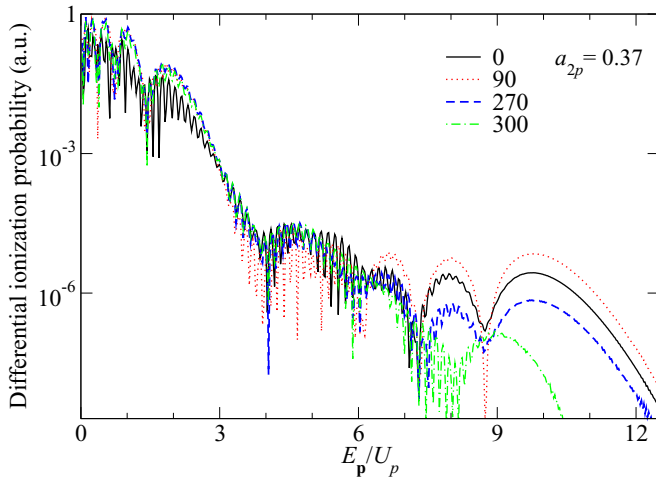
FIG. 3. Differential ionization probabilities of the He atom in a coherent superposition of the $2s$ and $2p$ states, with $a_{2p} = 0.37$ and the relative phase φ_{2p} (in degrees) labeled in the legend, as functions of the photoelectron energy $E_{\mathbf{p}}$ in units of the ponderomotive energy U_p. The laser pulse is sine squared with the carrier-envelope phase $\varphi = 0$ and the total pulse duration of six optical cycles. The laser wavelength and intensity are 3100 nm and 3×10^{12} W/cm², respectively. The results are obtained using the ISFA.
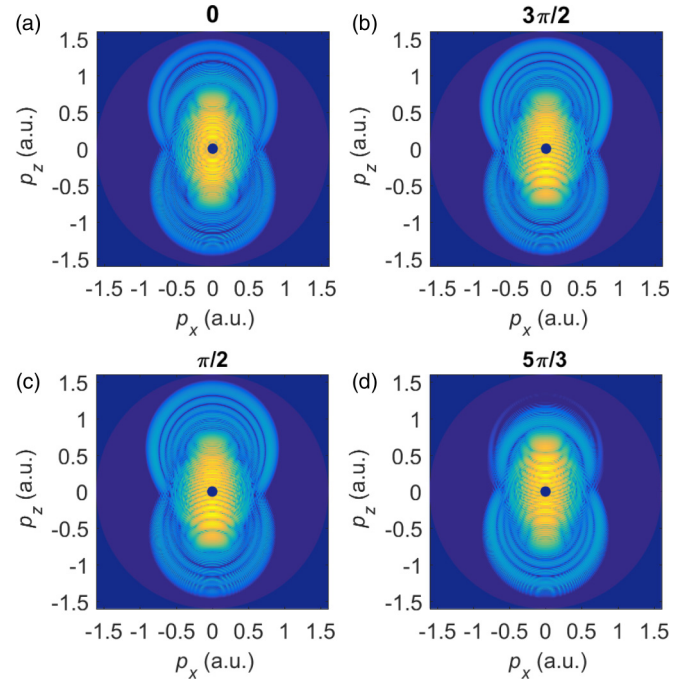

FIG. 4. Logarithm of the differential ionization probabilities of the He atom in a coherent superposition of the $2s$ and $2p$ states, with $a_{2p} = 0.37$ and the relative phase φ_{2p} equal to (a) 0, (b) $3\pi/2$, (c) $\pi/2$, and (d) $5\pi/3$, presented in the photoelectron momentum plane using false colors with the color scale that covers approximately seven orders of magnitude. The laser pulse parameters are the same as in Fig. 3 and the results are obtained using the ISFA.

exponentially decreasing part of the spectrum corresponds to the electrons which go directly to the detector (the Coulomb effects can change this part of the spectrum inducing low-energy structures caused by forward-scattered electrons; for more about the Coulomb effects in ATI, see the recent review article [63]). This low-energy part is followed by a plateau which extends approximately from $3U_p$ to $10U_p$ and is lower by many orders of magnitude. This plateau corresponds to the electrons which, virtually liberated in the atomic ionization, are driven by the laser field and return to and rescatter off the ionic core (this is in accordance with the three-step model). For energies larger than $10U_p$ the photoelectron yield again exponentially decreases (this is the so-called cutoff). The photoelectron momentum distribution has a figure-8 form, elongated along the polarization axis, with different off-axis structures which have exotic names such as spider, rhomb, fork, and carpet.

Let us now present the ISFA numerical results for the differential ionization probabilities of the He atom in the coherent superposition of the $2s$ and $2p$ states with the amplitudes $a_{2p} = 0.37$ and $a_{2s} = (1 - a_{2p}^2)^{1/2}$, fixed phase $\varphi_{2s} = 0$, and various values of the phase φ_{2p}. For the chosen amplitudes the contributions of the $2s$ and $2p$ states to the differential ionization probability are comparable. The laser pulse is sine squared and is given by Eqs. (3) and (4) with the carrier-envelope phase $\varphi_R \rightarrow \varphi$. The laser wavelength and intensity are 3100 nm and 3×10^{12} W/cm², respectively, the total pulse duration is six cycles, and the carrier-envelope phase is $\varphi = 0$. These parameters are close to that of a recent experiment [64] with the Cs atom, which has an ionization potential of 3.9 eV, which is close to $I_p(2s) = 3.972$ eV. Since the wavelength used is nonresonant, the states $2s$ and $2p$ are not coupled and the coefficients $c_j = a_j e^{i\varphi_j}$ do not depend on time.

In Fig. 3 we present the spectra for emission in the laser-field polarization direction $\theta = 0$ for the relative phases $\varphi_{2p} = 0°$, $90°$, $270°$, and $300°$. We see that the results strongly depend on the value of this phase. Due to its lower ionization potential, the ionization probability of the $2p$ state is higher than that of the $2s$ state. However, the relative amplitude of these states in our coherent superposition is chosen such that the corresponding ionization amplitudes are comparable. Therefore, the contributions from the $2s$ and $2p$ states interfere constructively or destructively, depending on the relative phase φ_{2p}, and produce different spectra, as can be seen in Fig. 3.

In Fig. 4 we present the photoelectron momentum distributions for the same parameters as in Fig. 3. We see that both the low-energy (direct electrons) and high-energy (rescattered electrons) spectra strongly depend on the relative phase φ_{2p}. As we have mentioned, this phase can be controlled in the experiment by choosing the carrier-envelope phase φ_R of our weak resonant laser pulse [taking into account that the wave functions are determined up to a phase factor, the connection is $\varphi_{2p} = -\varphi_R + \pi/2$; see Eq. (15)].

V. STRONG RESONANT LASER PULSE

In Appendix B we explore how the ionization rates depend on the ionization potential I_p and the laser-field intensity I and frequency ω. We estimate that, for an experimental observation of novel effects in strong-field ionization from a coherent superposition of states, the most suitable example
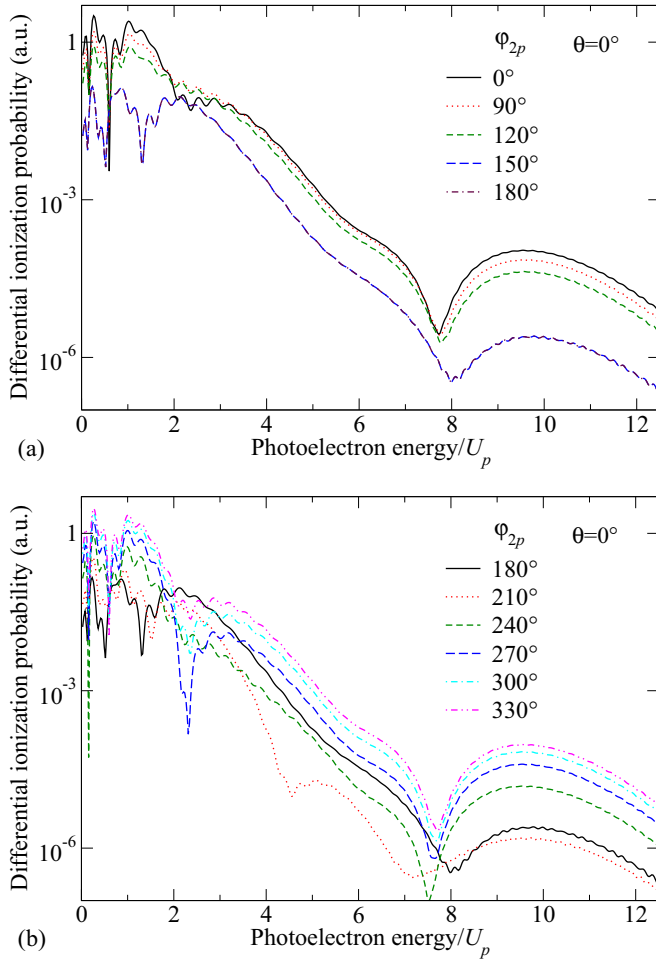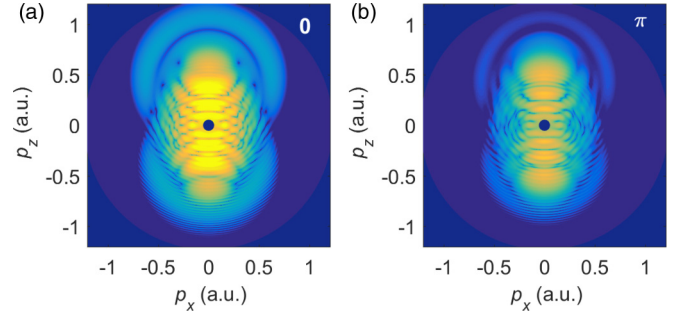
FIG. 6. Logarithm of the differential ionization probabilities of the He atom in a coherent superposition of the $2s$ and $2p$ states, presented in the photoelectron momentum plane using false colors with a color scale that covers six orders of magnitude. The relative phase is (a) $\varphi_{2p} = 0$ and (b) $\varphi_{2p} = \pi$. The laser pulse parameters are as in Fig. 5.

FIG. 5. Differential ionization probabilities for HATI of the He atom in a coherent superposition of the $2s$ and $2p$ states, with $a_{2p} = 0.37$, $a_{2s}^2 + a_{2p}^2 = 1$, $\varphi_{2s} = 0$, and φ_{2p} (a) from 0 to 180° and (b) from 180° to 330°, as functions of the photoelectron energy $E_\mathbf{p}$ in units of the ponderomotive energy U_p. A linearly polarized four-cycle sine-squared laser pulse with a carrier-envelope phase $\varphi = 0$, a wavelength of 2057 nm, and an intensity of 4×10^{12} W/cm^2 is used. The electrons are emitted in the laser-field polarization direction ($\theta = 0°$).

is the superposition of the $2s$ and $2p$ excited states of the He atom exposed to a laser field having an intensity of few units of 10^{12} W/cm^2 and a resonant wavelength 2057 nm (one photon resonance). Therefore, in this section we suppose that the laser field is resonant with the transition from the $2s$ state to the $2p$ state. In order to have comparable contributions of the $2s$ and $2p$ states to the ionization amplitude we choose $a_{2p} = 0.37$ and $a_{2s}^2 + a_{2p}^2 = 1$. We fix the phase of the $2s$ state $\varphi_{2s} = 0$ and change the phase φ_{2p} of the $2p$ state.

A. ISFA results

The laser pulse is turned on at the time $t = 0$ when the initial bound state is $\psi(0) = a_{2s}\psi_{2s} + a_{2p}e^{i\varphi_{2p}}\psi_{2p}$. Since the laser pulse is resonant, we can suppose that the bound atomic states evolve from the time $t = 0$ to the ionization time $t = t_0$ in accordance with the two-level model described in Sec. II. In this case the bound atomic state is given by Eq. (23), where

the coefficients $c_j(t)$ are given by

$$c_{2s}(t) = a_{2s}\cos[F(t)] - ia_{2p}\sin[F(t)]e^{i(\varphi + \varphi_{2p})},$$
$$c_{2p}(t) = a_{2p}\cos[F(t)]e^{i\varphi_{2p}} - ia_{2s}\sin[F(t)]e^{-i\varphi}, \quad (24)$$

with $F(t) = -3n_p E_0[\omega t/n_p - \sin(\omega t/n_p)]/4\omega$. Equations (21)–(23), with (24), constitute our modified ISFA which we will use in this section.

Let us first analyze how the photoelectron spectra depend on the relative phase between the states in the coherent superposition of the $2s$ and $2p$ states. In Fig. 5 we present the results for a laser intensity of 4×10^{12} W/cm^2, a wavelength of 2057 nm, and the four-cycle sine-squared pulse with the carrier-envelope phase $\varphi = 0$ [compare Eqs. (3) and (4) for $\varphi_R \to \varphi$]. We see that the spectra strongly depend on the value of the relative phase φ_{2p}. The differential ionization probability is maximal for $\varphi_{2p} \approx 0°$ and slowly decreases with the increase of φ_{2p}. For $\varphi_{2p} > 90°$ the decrease of the probability with the increase of φ_{2p} is faster. The minimum appears for $\varphi_{2p} \approx 180°$. This is followed by a fast increase of the rate with the increase of φ_{2p} from 180° to 270° and a slower increase for $\varphi_{2p} > 270°$.

In Fig. 6 we present the photoelectron momentum distributions for the same laser pulse parameters as in Fig. 5. Due to a short pulse duration, the momentum distributions exhibit known asymmetry along the polarization axis ($\theta = 0°$ vs $\theta = 180°$ [59]). We see that the ionization probability is higher for $\varphi_{2p} = 0$ [Fig. 6(a)] than for $\varphi_{2p} = \pi$ [Fig. 6(b)].

It is known that for long pulses (say, $T_p > 10T$) the photoelectron spectra do not depend on the carrier-envelope phase and that they can be approximated by the spectra obtained using a T-periodic infinitely long flat pulse [59]. We have checked that this is valid for ionization from the $2s$ and $2p$ states alone. However, for ionization from a coherent superposition of states this is not so. This is obvious from the results presented in Fig. 7: The results for $\varphi = 0°$ and $-180°$ differ by more than one order of magnitude (for some energies this difference is by a factor larger than 30). Therefore, by measuring the differential ionization probability from a coherent superposition of states, one can determine the phase φ. This is a different method for measurement of the carrier-envelope phase. It can be used for long pulses and for arbitrary electron
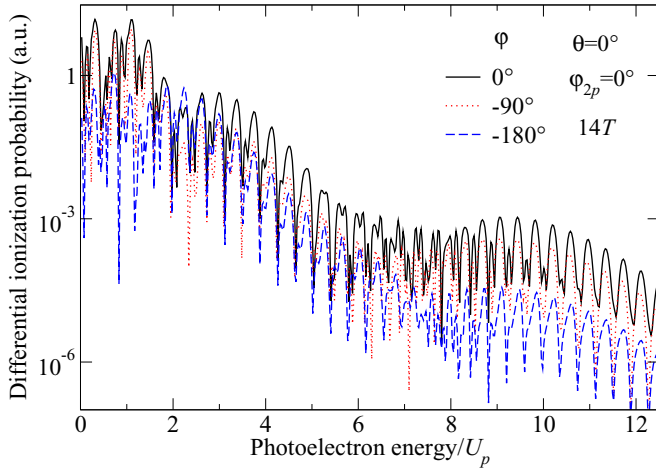
FIG. 7. Differential ionization probabilities of the excited He atom as functions of the photoelectron energy $E_\mathbf{p}$ in units of the ponderomotive energy U_p for above-threshold ionization by a linearly polarized sine-squared laser pulse of the total duration $T_p = 14T$ having a wavelength of 2057 nm ($E_{2p} - E_{2s} = \omega$) and an intensity of 4×10^{12} W/cm^2. The electrons are emitted in the laser-field polarization direction ($\theta = 0°$). Ionization is from a coherent superposition of the 2s and 2p states, with $a_{2p} = 0.37$, $a_{2s}^2 + a_{2p}^2 = 1$, and $\varphi_{2s} = \varphi_{2p} = 0$. The results for the carrier-envelope phases $\varphi = 0°$, $-90°$, and $-180°$, are presented.

emission angles. This method can be used instead of the known stereo-ATI method [59,65].

B. TDSE results

In this section we present numerical results obtained using the solutions of the time-dependent Schrödinger equation as it is described in Sec. III. We take the initial state in the form of a superposition of the $\psi_{2s}(\mathbf{r})$ and $\psi_{2p}(\mathbf{r})$ states:

$$\Psi(\mathbf{r}, 0) = a_{2s}\psi_{2s}(\mathbf{r}) + a_{2p}e^{i\varphi_{2p}}\psi_{2p}(\mathbf{r}). \quad (25)$$

In Fig. 8 we compare the results for $\varphi_{2p} = 0$ and $\varphi_{2p} = \pi$ for the four-cycle sine-squared pulse with the carrier-envelope phase $\varphi = 0$, a wavelength of 2057 nm, and intensities of 2×10^{12} W/cm^2 [Fig. 8(a)] and 4×10^{12} W/cm^2 [Fig. 8(b)]. For an intensity of 2×10^{12} W/cm^2 the ionization probability in the low-energy region is larger for $\varphi_{2p} = 0$, while for high energies the situation is the opposite. For two times higher intensity [Fig. 8(b)] the spectra change qualitatively: Now the ionization probability for $\varphi_{2p} = 0$ is higher in the plateau and cutoff region, while in the low-energy region the probabilities for $\varphi_{2p} = 0$ and $\varphi_{2p} = \pi$ are comparable. Comparing the TDSE results with the results obtained using the ISFA (Fig. 5), we see that the agreement is good (having in mind that the SFA fails in the low-energy region due to the neglect of the Coulomb effects).

In Fig. 9 we present the survival probabilities of the 2s and 2p states as functions of time during the laser pulse, for ionization by the laser pulse with an intensity of 4×10^{12} W/cm^2 and other parameters as in Fig. 8. We see that both survival probabilities oscillate. Interestingly, in most cases the maxima in survival probability appear each half cycle, at the times when the field has an extremum. The 2s state survival
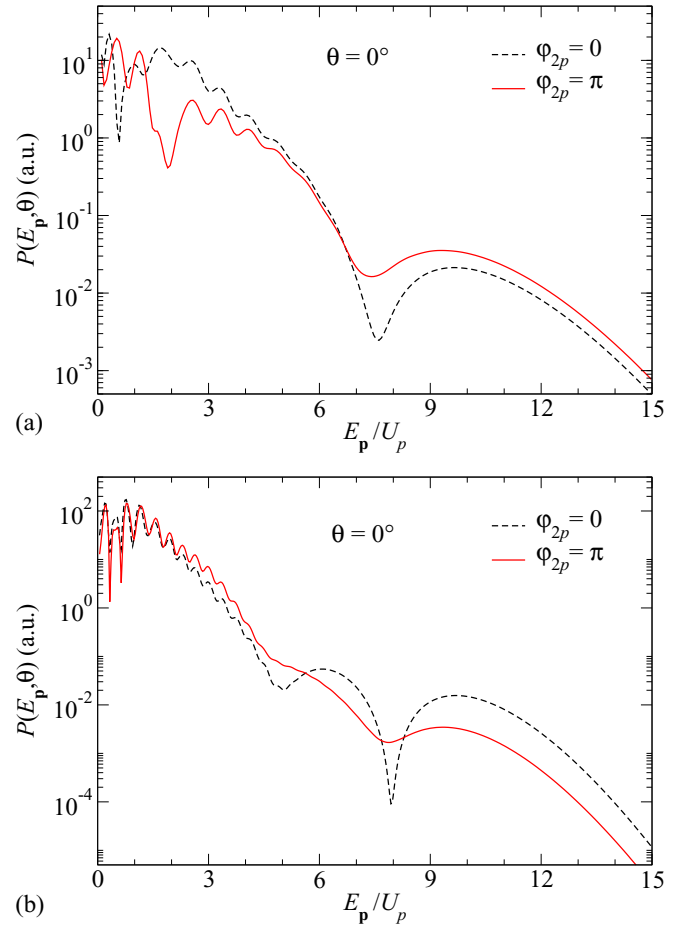

FIG. 8. Differential ionization probabilities of the He atom in a coherent superposition of the 2s and 2p states, with $a_{2p} = 0.37$, $a_{2s}^2 + a_{2p}^2 = 1$, $\varphi_{2s} = 0$, and $\varphi_{2p} = 0$ (black dashed curve) and $\varphi_{2p} = \pi$ (red solid curve). The ionization is by a linearly polarized four-cycle sine-squared pulse with the carrier-envelope phase $\varphi = 0$, wavelength 2057 nm, and intensities (a) 2×10^{12} W/cm^2 and (b) 4×10^{12} W/cm^2. The electrons are emitted in the laser-field polarization direction. The results are obtained using the TDSE solutions.

probability decreases and at the end of the pulse the survival probability of the 2p state is larger than that of the 2s state.

VI. DISCUSSION AND CONCLUSIONS

Using radiation from a free-electron-laser or a high-harmonic source, we first excited the ground atomic state. For example, for the 1s ground state of the helium atom the selection rules allow transition to a p state. In this way we obtained the He atomic gas in the 2p excited state. In order to prepare a coherent superposition of the 2s and 2p bound states of the He atom we used a weak resonant laser pulse having a wavelength of 2057 nm. Using the two-level model, we have shown that the relative phase between the states in this coherent superposition of states depends on the carrier-envelope phase of the weak resonant laser pulse used, while the corresponding relative amplitude is equal to $\tan(F_p)$, where $F_p = 0.75T_p\sqrt{I}$, with T_p the total pulse duration and I the laser intensity [see Eq. (15)]. The validity of our two-level model was confirmed using the exact TDSE solutions.
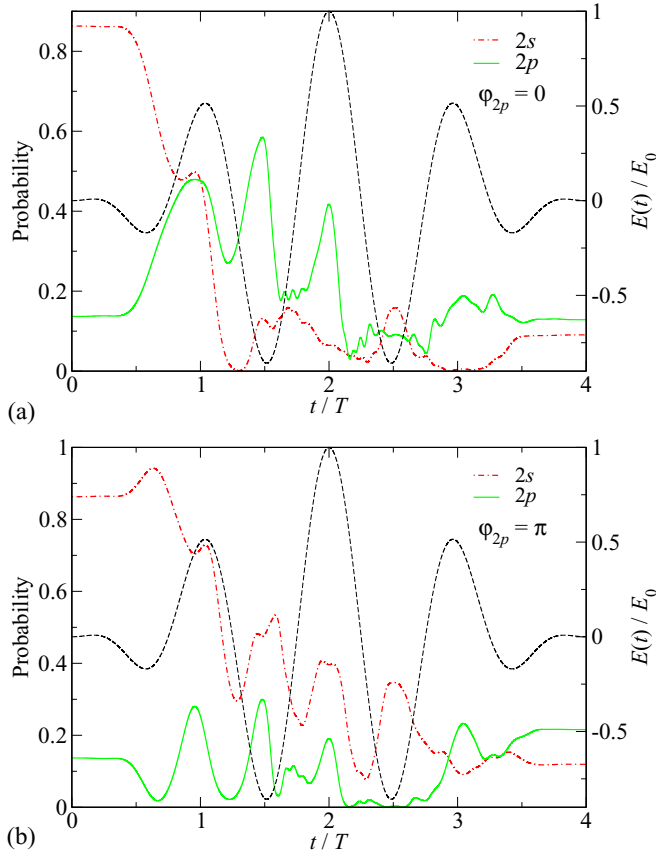
FIG. 9. Survival probabilities of the $2s$ (red dot-dashed lines) and $2p$ (green solid lines) states as functions of the time in ionization from the coherent superposition of these states for (a) $\varphi_{2p} = 0$ and (b) $\varphi_{2p} = \pi$ and for the parameters of Fig. 8 and a laser intensity of 4×10^{12} W/cm^2. The laser electric-field vector is presented on the right-hand ordinate by a black dashed line.

After preparing a coherent superposition of states with controlled relative amplitude and phase, we considered strong-laser-field-induced ionization from such a superposition. We separately examined the cases of nonresonant and resonant intense laser fields. For ionization by a strong nonresonant few-cycle pulse, the photoelectron spectra and the momentum distributions strongly depend on the relative phase of the states in the coherent superposition. The differential ionization probability of the high-energy plateau and cutoff electrons can differ by orders of magnitude for different values of this relative phase. We expect that some additional information about the ionization process can be deduced from these photoelectron spectra and the momentum distributions. For example, information about the ionization time, which may be different for the $2s$ and $2p$ states, can be tracked by changing the relative phase between these states. We have shown that this relative phase is equal to $\varphi_R - \pi/2$ and can be controlled by changing the carrier-envelope phase φ_R of the weak resonant pulse which generates this coherent superposition.

We have also considered the case of ionization by a strong resonant laser field. For this purpose we modified our ISFA theory for the resonant case. It is known that the carrier-envelope phase of a few-cycle pulse can be determined by

measuring the asymmetry in the photoelectron yield in the two opposite directions (the so-called stereo-ATI method). This works well for short pulses and high photoelectron energies. For pulses longer than ten optical cycles this asymmetry becomes negligibly small. The above conclusions are valid for the ATI from a single state. However, for the ATI from a coherent superposition of states the influence on the carrier-envelope phase is much more pronounced and is strong even for long pulses. In this case the carrier-envelope phase can be determined using the spectra for a fixed photoelectron emission angle for which the time-of-flight method with only one detector can be used to record the photoelectron spectrum. The strong-field ionization is moving rapidly into the mid-IR region, and typical mid-IR pulses are long (i.e., many-cycle). The presented results show how our proposed method can be used to determine the carrier-envelope phase of a mid-IR pulse, which is of interest for the new trends in laser-matter interactions.

In conclusion, we have shown how it is possible to prepare a coherent superposition of states with controllable relative amplitude and phase of these states. We have developed the ISFA theory of HATI from a superposition of the bound atomic states, for both the nonresonant and resonant cases of the ionizing intense laser field. Our numerical results, confirmed by using the exact TDSE solutions, show that the photoelectron spectra and the momentum distributions strongly depend on the mentioned relative amplitude and phase. Furthermore, in the resonant case the ionization amplitude depends strongly on the carrier-envelope phase of the intense laser pulse used, so the HATI from the coherent superposition of states can be used for the measurement of this phase. This is valid even for long pulses, where other methods, such as stereo-ATI, fail, so the strong-field ionization from a coherent superposition of states may be a unique method for measurement of the carrier-envelope phase of long laser pulses.

A suggested experiment would be done by means of three relatively delayed pulses in a pump-control-probe manner. First, an XUV pulse transfers the He ground state to the He* $2p$ state via one-photon-absorption process. After the XUV pulse is gone, a weak resonant laser pulse creates a coherent superposition of the $2p$ and $2s$ states, whose relative phase and amplitudes can be controlled by means of the carrier-envelope phase and laser intensity. In the third step, a strong laser probe arrives after the controlling pulse is gone. In this work we discuss several options for the probe pulse. In one case, labeled as resonant, the probe can be the same wavelength as the one used for the control pulse. In the second case we discuss, the probe pulse wavelength is not resonant with the $2p$-$2s$ transition.

In our work we considered analytically the simple case of a sine-squared pulse. For a Gaussian pulse with the intensity distribution $I(t) = I_{\max} e^{-t^2/\tau_g^2}$, we can use the fact that the function $\sin^4(\pi t/4.75)$ is fitted well with the function e^{-t^2}. From this we estimate that $T_p = 4.75\tau_g$ (the pulse duration time usually used in the experiment is $\tau_p = 2\sqrt{\ln 2}\tau_g \approx \tau_g/0.6$). Therefore, our method can be useful for pulse-shape characterization, since, although Gaussian, the pulse shape is not necessarily precisely known in the experiment [for

a Gaussian pulse, the result for $F(t)$, Eq. (10), is $F(t) = \mu\sqrt{\pi/2}\tau_g \text{erf}(t/\sqrt{2}\tau_g)]$.

APPENDIX A: DIPOLE MATRIX ELEMENTS

Our S-matrix element is expressed as a double integral over the ionization and travel times of highly oscillatory functions. For fast calculations we need an analytical form of the subintegral function, which contains a product of the dipole matrix elements. For the initial hydrogen-like atomic state wave function $\psi_{n\ell m}^{\alpha_{n\ell}}(\mathbf{r})$, $\alpha_{n\ell}^2 = 2I_p(n\ell)$, with $I_p(n\ell)$ the ionization potential; the dipole matrix element is $\langle \mathbf{q}|\mathbf{r}|\psi_{n\ell m}^{\alpha_{n\ell}}\rangle = i\partial\phi_{n\ell m}^{\alpha_{n\ell}}(\mathbf{q})/\partial\mathbf{q} = i(\hat{\mathbf{e}}_q\frac{\partial}{\partial q} + \hat{\mathbf{e}}_{\theta_q}\frac{1}{q}\frac{\partial}{\partial\theta_q} + \hat{\mathbf{e}}_{\phi_q}\frac{1}{q\sin\theta_q}\frac{\partial}{\partial\phi_q})\phi_{n\ell m}^{\alpha_{n\ell}}(\mathbf{q})$, where (q, θ_q, ϕ_q) are the spherical coordinates and $\phi_{n\ell m}^{\alpha_{n\ell}}(\mathbf{q})$ are the momentum-space hydrogenic wave functions, which (up to a phase factor) can be expressed via the Gegenbauer polynomial $C_{n-\ell-1}^{\ell+1}$ and the spherical harmonic $Y_{\ell m}$ [66],

$$\phi_{n\ell m}^{\alpha_{n\ell}}(\mathbf{q}) = \left[\frac{2}{\pi}\frac{n(n-\ell-1)!}{(n+\ell)!}\right]^{1/2}(-i)^\ell 2^{2\ell+2}\ell!\,\alpha_{n\ell}^{\ell+5/2}$$
$$\times \frac{q^\ell Y_{\ell m}(\hat{\mathbf{e}}_q)}{(q^2+\alpha_{n\ell}^2)^{\ell+2}}C_{n-\ell-1}^{\ell+1}\left(\frac{q^2-\alpha_{n\ell}^2}{q^2+\alpha_{n\ell}^2}\right). \quad (A1)$$

For the ns state we have $\ell = m = 0$ and $Y_{00}(\hat{\mathbf{e}}_q) = 1/\sqrt{4\pi}$, while for the np states we have $\ell = 1$, $m = 0$, and $Y_{10}(\hat{\mathbf{e}}_q) = \sqrt{\frac{3}{4\pi}}\cos\theta_q$. For a laser field which is linearly polarized along the $\hat{\mathbf{e}}_z$ axis, $\mathbf{E}(t) = E(t)\hat{\mathbf{e}}_z$; in spherical coordinates we have $\hat{\mathbf{e}}_q\cdot\hat{\mathbf{e}}_z = \cos\theta_q$ and $\hat{\mathbf{e}}_{\theta_q}\cdot\hat{\mathbf{e}}_z = -\sin\theta_q$.

Since $\phi_{n00}^{\alpha_{n0}}(\mathbf{q})$ does not depend on the angles (θ_q, φ_q), using the notation $y = q^2$, $x_{n0} = 1/(y + \alpha_{n0}^2)$, and $z_{n0} = (y - \alpha_{n0}^2)x_{n0}$, we obtain

$$\langle \mathbf{q}|\mathbf{r}\cdot\hat{\mathbf{e}}_z|\psi_{n00}^{\alpha_{n0}}\rangle = i\frac{q_z}{q}\frac{\partial\phi_{n00}^{\alpha_{n0}}}{\partial q} = c_{n0}q_z F_{n0}(q), \quad (A2)$$

where $F_{n0}(q) = -d[x_{n0}^2 C_{n-1}^1(z_{n0})]/dy = x_{n0}^3 C_{n-1}^1(z_{n0}) - 2\alpha_{n0}^2 x_{n0}^4 C_{n-2}^2(z_{n0})$, $c_{n0} = -i(2\alpha_{n0})^{5/2}/\pi$, and we used the relation $dC_n^\lambda(z)/dz = 2\lambda C_{n-1}^{\lambda+1}(z)$ [67]. Using the relations [66] $C_0^\lambda(z) = 1$, $C_1^\lambda(z) = 2\lambda z$ [$\lambda \neq 0$ and $C_1^0(z) = 2z$], $C_2^\lambda(z) = 2\lambda(\lambda+1)z^2 - \lambda$, and $C_3^\lambda(z) = -2(1+\lambda)\lambda z + 4\lambda(1+\lambda)(2+\lambda)z^3/3$, for $n = 1, 2, 3, 4$ we get

$$F_{10}(q) = 2x_{10}^3, \quad F_{20}(q) = 4(q^2 - 2\alpha_{20}^2)x_{20}^4,$$
$$F_{30}(q) = 2(3q^4 - 18\alpha_{30}^2 q^2 + 11\alpha_{30}^4)x_{30}^5,$$
$$F_{40}(q) = 8(q^6 - 12\alpha_{40}^2 q^4 + 21\alpha_{40}^4 q^2 - 6\alpha_{40}^6)x_{40}^6. \quad (A3)$$

For the np state we have

$$\langle \mathbf{q}|\mathbf{r}\cdot\hat{\mathbf{e}}_z|\psi_{n10}^{\alpha_{n1}}\rangle = c_{n1}\left(\frac{dF_{n1}}{dq}\cos^2\theta_q + \frac{F_{n1}}{q}\sin^2\theta_q\right), \quad (A4)$$

where $c_{n1} = (2\alpha_{n1})^{7/2}\sqrt{3}/(\pi\sqrt{n^2-1})$ and $F_{n1}(q) = qx_{n1}^3 C_{n-2}^2(z_{n1})$. In particular, for $n = 2, 3, 4$ we get

$$F_{21}(q) = qx_{21}^3, \quad F_{31}(q) = 4q(q^2 - \alpha_{31}^2)x_{31}^4,$$
$$F_{41}(q) = 2q[6(q^2 - \alpha_{41}^2)^2 - (q^2 + \alpha_{41}^2)^2]x_{41}^5,$$
$$dF_{21}/dq = (\alpha_{21}^2 - 5q^2)x_{21}^4,$$
$$dF_{31}/dq = 4(10q^2\alpha_{31}^2 - \alpha_{31}^4 - 5q^4)x_{31}^5,$$
$$dF_{41}/dq = \{2(\alpha_{41}^2 - 5q^2)[6(q^2 - \alpha_{41}^2)^2 - (q^2 + \alpha_{41}^2)^2]$$
$$+ 96\alpha_{41}^2 q^2(q^2 - \alpha_{41}^2)\}x_{41}^6. \quad (A5)$$

APPENDIX B: ESTIMATION OF THE PARAMETERS

Let us estimate the laser parameters relevant for the observation of the interference of different contributions to the strong-field ionization from a coherent superposition of excited atomic states. We consider the nj excited states of the He atom, with the corresponding ionization potentials $I_p(nj)$ for $n = 2, 3, 4$ and $j = s, p$.

The appearance intensity is the laser intensity at which the ionization becomes noticeable, while the saturation intensity is the laser intensity at which almost all atoms of the considered gaseous medium are ionized. The appearance and saturation intensities for arbitrary atomic states can be estimated using the known ionization potentials and appearance and saturation intensities for noble-gas atoms. The quasistatic Ammosov-Delone-Krainov tunneling rate (see [9] and references therein) is given by an exponential function with the factor $\xi = \sqrt{I_p^3/I}$ in the exponent. In Table I we present the ionization potentials I_p and the appearance and saturation intensities for the ground state of noble gases, taken from [68], as well as the corresponding values of the parameter ξ. The value of this parameter does not change much for different noble gases. We suppose that this parameter has the same value for the excited states of the He atom. Therefore, we have $I_{\text{sat}}^{nj} = [I_p(nj)/I_p]^3 I_{\text{sat}}$ and an analogous relation for the appearance intensities. In the last 12 columns of Table I we present the so-estimated values of I_{app}^{nj} and I_{sat}^{nj} for $n = 2, 3, 4$ and $j = s, p$. Using these results, we can estimate the laser intensities for which a pair of the excited states of He takes part in the strong-field-ionization process.

The energy difference between the He $1s$ ground state and the excited states is large, so the appearance intensity for the $1s$ state is much larger than the saturation intensity for the excited states. Therefore, the required strong-field ionization from a coherent superposition should be realized using excited states. In this case, the ground state is not involved in the strong-field ionization. It is only used in the pump process in which, as we have mentioned in the Introduction, we can use high-harmonic or free-electron-laser radiation to excite the $1s$ state and populate the p states (selection rules allow the transition $1s \to np$). However, the difference between the ionization potentials $I_p(np)$ and $I_p(n+1p)$, $n = 2, 3$, is large,

TABLE I. Ionization potentials I_p, appearance intensities I_{app}, saturation intensities I_{sat}, and the parameters $\xi_{app} = \sqrt{I_p^3/I_{app}}$ and $\xi_{sat} = \sqrt{I_p^3/I_{sat}}$ (in a.u.) of the ground state of noble gases [68]. The corresponding intensities I_{app}^{nj} and I_{sat}^{nj} ($n = 2, 3, 4$ and $j = s, p$) for the excited states of the He atom are also shown. Intensities are in units of 10^{11} W/cm^2. The ionization potentials for the excited states of He atom are [69] $I_p(2s) = 3.972$ eV, $I_p(3s) = 1.667$ eV, $I_p(4s) = 0.9138$ eV, $I_p(2p) = 3.369$ eV, $I_p(3p) = 1.500$ eV, $I_p(4p) = 0.8454$ eV.

Atom	I_p (eV)	I_{app}	I_{sat}	ξ_{app}	ξ_{sat}	I_{app}^{2s}	I_{sat}^{2s}	I_{app}^{2p}	I_{sat}^{2p}	I_{app}^{3s}	I_{sat}^{3s}	I_{app}^{3p}	I_{sat}^{3p}	I_{app}^{4s}	I_{sat}^{4s}	I_{app}^{4p}	I_{sat}^{4p}
He	24.59	2500	15000	10.18	4.155	10.5	63.2	6.43	38.6	0.779	4.67	0.567	3.40	0.128	0.770	0.102	0.610
Ne	21.56	2000	8300	9.342	4.586	12.5	51.9	7.63	31.7	0.924	3.84	0.674	2.80	0.152	0.632	0.121	0.500
Ar	15.76	200	2000	18.46	5.839	3.20	32.0	1.95	19.5	0.237	2.37	0.172	1.72	0.0390	0.390	0.0309	0.309
Kr	14.00	160	1300	17.28	6.063	3.65	29.7	2.23	18.1	0.270	2.19	0.197	1.60	0.0445	0.362	0.0352	0.286
Xe	12.13	40	700	27.88	6.664	1.40	24.6	0.857	15.0	0.104	1.82	0.0756	1.32	0.0171	0.299	0.237	0.237

so that the corresponding ionization probabilities can differ by orders of magnitude and it would be difficult to observe the interference of the corresponding amplitudes, which is the aim of our work. For example, let us consider the strong-field ionization from a coherent superposition of the $2p$ and $3p$ states by the laser field having an intensity of 5×10^{11} W/cm^2 and a resonant wavelength of 6634 nm ($E_{3p} - E_{2p} = 10\omega$). In this case, in order to have noticeable interference effects of the ionization amplitudes of the $2p$ and $3p$ states, the coefficient a_{3p} should be very small (our calculations give $a_{3p} = 0.000\,21$ and $a_{2p}^2 + a_{3p}^2 = 1$). The reason is the large difference in the ionization potentials of the $2p$ and $3p$ states $(3.369 - 1.500 = 1.869$ eV), which causes the difference between the ionization probabilities from these states alone to be many orders of magnitude. For the $3p$ and $4p$ states this difference is smaller $(1.500 - 0.8454 = 0.6546$ eV). For the coherent superposition of the $3p$ and $4p$ states we can use an intensity of $I \approx 10^{11}$ W/cm^2 since it is only slightly above the saturation intensity for the $4p$ states but is well above the

appearance intensity for the $3p$ state. We are interested in the rescattering plateau which extends up to $10U_p$, $U_p = I/4\omega^2$. For an intensity of 1×10^{11} W/cm^2 and a wavelength of 10 000 nm, $10U_p$ is equal to 9.34 eV. Therefore, in order to observe the effect of the superposition of $3p$ and $4p$ states in the photoelectron energy region of tens of eV, lasers with wavelengths longer than 10 000 nm should be used. An example is the resonant wavelength of 11 365 nm ($E_{4p} - E_{3p} = 6\omega$). In this case our calculations show that the desired interference can be obtained for $a_{4p} = 0.019$.

The difference between the ionization potentials of the $2s$ and $2p$ states is 0.603 eV, which corresponds to the resonant wavelength of 2057 nm. According to Table I, one expects the interference effects in strong-field ionization from a coherent superposition of the $2s$ and $2p$ states for a wide interval of laser intensities of a few times 10^{12} W/cm^2. These intensities and wavelengths are nowadays commonly used in strong-field physics. Therefore, we considered this example in the present paper.

[1] D. B. Milošević and F. Ehlotzky, Scattering and reaction processes in powerful laser fields, Adv. At. Mol. Opt. Phys. **49**, 373 (2003).

[2] F. Krausz and M. Ivanov, Attosecond physics, Rev. Mod. Phys. **81**, 163 (2009).

[3] S. Grundmann, D. Trabert, K. Fehre, N. Strenger, A. Pier, L. Kaiser, M. Kircher, M. Weller, S. Eckart, L. P. H. Schmidt, F. Trinter, T. Jahnke, M. S. Schöffler, and R. Dörner, Zeptosecond birth time delay in molecular photoionization, Science **370**, 339 (2020).

[4] P. Salières, A. L'Huillier, P. Antoine, and M. Lewenstein, Study of the spatial and temporal coherence of high-order harmonics, Adv. At. Mol. Phys. **41**, 83 (1999).

[5] M. B. Gaarde, J. L. Tate, and K. J. Schafer, Macroscopic aspects of attosecond pulse generation, J. Phys. B **41**, 132001 (2008).

[6] F. Calegari, F. Ferrari, M. Lucchini, M. Negro, C. Vozzi, S. Stagira, G. Sansone, and M. Nisoli, Principles and applications of attosecond technology, Adv. At. Mol. Phys. **60**, 371 (2011).

[7] M. C. Kohler, T. Pfeifer, K. Z. Hatsagortsyan, and C. H. Keitel, Frontiers of atomic high-harmonic generation, Adv. At. Mol. Opt. Phys. **61**, 159 (2012).

[8] A.-T. Le, H. Wei, C. Jin, and C. D. Lin, Tutorial: Strong-field approximation and its extension for high-order harmonic generation with mid-infrared lasers, J. Phys. B **49**, 053001 (2016).

[9] W. Becker, F. Grasbon, R. Kopold, D. B. Milošević, G. G. Paulus, and H. Walther, Above-threshold ionization: From classical features to quantum effects, Adv. At. Mol. Opt. Phys. **48**, 35 (2002).

[10] A. Becker and F. H. M. Faisal, Intense field many-body S-matrix theory, J. Phys. B **38**, R1 (2005).

[11] P. Agostini and L. F. DiMauro, Atomic and molecular ionization dynamics in strong laser fields: From optical to x-rays, Adv. At. Mol. Opt. Phys. **61**, 117 (2012).

[12] W. Becker, S. P. Goreslavski, D. B. Milošević, and G. G. Paulus, The plateau in above-threshold ionization: The keystone of rescattering physics, J. Phys. B **51**, 162002 (2018).

[13] C. F. de Morisson Faria and X. Liu, Electron-electron correlation in strong laser fields, J. Mod. Opt. **58**, 1076 (2011).

[14] W. Becker, X. J. Liu, P. J. Ho, and J. H. Eberly, Theories of photoelectron correlation in laser-driven multiple atomic ionization, Rev. Mod. Phys. **84**, 1011 (2012).

[15] P. Johnsson, J. Mauritsson, T. Remetter, A. L'Huillier, and K. J. Schafer, Attosecond Control of Ionization by Wave-Packet Interference, Phys. Rev. Lett. **99**, 233001 (2007).

[16] L. H. Haber, B. Doughty, and S. R. Leone, Continuum phase shifts and partial cross sections for photoionization from excited states of atomic helium measured by high-order harmonic

optical pump-probe velocity map imaging, Phys. Rev. A **79**, 031401(R) (2009).

[17] P. Ranitovic, X. M. Tong, B. Gramkow, S. De, B. DePaola, K. P. Singh, W. Cao, M. Magrakvelidze, D. Ray, I. Bocharova, H. Mashiko, A. Sandhu, E. Gagnon, M. M. Murnane, H. Kapteyn, I. Litvinyuk, and C. L. Cocke, IR-assisted ionization of helium by attosecond extreme ultraviolet radiation, New J. Phys. **12**, 013008 (2010).

[18] P. Ranitovic, X. M. Tong, C. W. Hogle, X. Zhou, Y. Liu, N. Toshima, M. M. Murnane, and H. C. Kapteyn, Controlling the XUV Transparency of Helium Using Two-Pathway Quantum Interference, Phys. Rev. Lett. **106**, 193008 (2011).

[19] P. Ranitovic, C. W. Hogle, P. Riviére, A. Palacios, X. M. Tong, N. Toshima, A. Gonzáles-Castrillo, F. Martin, M. M. Murnane, and H. C. Kapteyn, Attosecond vacuum UV coherent control of molecular dynamics, Proc. Natl. Acad. Sci. USA **111**, 912 (2014).

[20] N. Mayer, P. Peng, D. M. Villeneuve, S. Patchkovskii, M. Ivanov, O. Kornilov, M. J. J. Vrakking, and H. Niikura, Population transfer to high angular momentum states in infrared-assisted XUV photoionization of helium, J. Phys. B **53**, 164003 (2020).

[21] S. Meister, A. Bondy, K. Schnorr, S. Augustin, H. Lindenblatt, F. Trost, X. Xie, M. Braune, R. Treusch, B. Manschwetus, N. Schirmel, H. Redlin, N. Douguet, T. Pfeifer, K. Bartschat, and R. Moshammer, Photoelectron spectroscopy of laser dressed atomic helium, Phys. Rev. A **102**, 062809 (2020).

[22] P. M. Paul, T. O. Clatterbuck, C. Lynga, P. Colosimo, L. F. DiMauro, P. Agostini, and K. C. Kulander, Enhanced High Harmonic Generation from an Optically Prepared Excited Medium, Phys. Rev. Lett. **94**, 113906 (2005).

[23] J. B. Watson, A. Sanpera, X. Chen, and K. Burnett, Harmonic generation from a coherent superposition of states, Phys. Rev. A **53**, R1962(R) (1996).

[24] A. Sanpera, J. B. Watson, M. Lewenstein, and K. Burnett, Harmonic-generation control, Phys. Rev. A **54**, 4320 (1996).

[25] Z. Zeng, R. Li, Y. Cheng, W. Yu, and Z. Xu, Resonance-enhanced high-order harmonic generation and frequency mixing in two-color laser field, Phys. Scr. **66**, 321 (2002).

[26] V. Averbukh, High-order harmonic generation by excited helium: The atomic polarization effect, Phys. Rev. A **69**, 043406 (2004).

[27] D. B. Milošević, Theoretical analysis of high-order harmonic generation from a coherent superposition of states, J. Opt. Soc. Am. B **23**, 308 (2006).

[28] I. A. Ivanov and A. S. Kheifets, Resonant enhancement of generation of harmonics, Phys. Rev. A **78**, 053406 (2008).

[29] H. Niikura, D. M. Villeneuve, and P. B. Corkum, Mapping Attosecond Electron Wave Packet Motion, Phys. Rev. Lett. **94**, 083003 (2005).

[30] R. Ganeev, M. Suzuki, M. Baba, and H. Kuroda, High-order harmonic generation from boron plasma in the extreme-ultraviolet range, Opt. Lett. **30**, 768 (2005).

[31] R. A. Ganeev, High-order harmonic generation in a laser plasma: A review of recent achievements, J. Phys. B **40**, R213 (2007).

[32] R. A. Ganeev, Generation of high-order harmonics of high-power lasers in plasmas produced under irradiation of solid target surfaces by a prepulse, Phys. Usp. **52**, 55 (2009).

[33] R. Ganeev, *Interaction of Mid-Infrared Parametric Waves in Laser Plasmas* (World Scientific, Singapore, 2017).

[34] D. B. Milošević, High-energy stimulated emission from plasma ablation pumped by resonant high-order harmonic generation, J. Phys. B **40**, 3367 (2007).

[35] R. A. Ganeev and D. B. Milošević, Comparative analysis of the high-order harmonic generation in the laser ablation plasmas prepared on the surfaces of complex and atomic targets, J. Opt. Soc. Am. B **25**, 1127 (2008).

[36] D. B. Milošević, Resonant high-order harmonic generation from plasma ablation: Laser intensity dependence of the harmonic intensity and phase, Phys. Rev. A **81**, 023802 (2010).

[37] V. Strelkov, Role of Autoionizing State in Resonant High-Order Harmonic Generation and Attosecond Pulse Production, Phys. Rev. Lett. **104**, 123901 (2010).

[38] R. R. Freeman, P. H. Bucksbaum, H. Milchberg, S. Darack, D. Schumacher, and M. E. Geusic, Above-Threshold Ionization with Subpicosecond Laser Pulses, Phys. Rev. Lett. **59**, 1092 (1987).

[39] M. P. de Boer and H. G. Muller, Observation of Large Populations in Excited States After Short-Pulse Multiphoton Ionization, Phys. Rev. Lett. **68**, 2747 (1992).

[40] R. R. Jones, D. W. Schumacher, and P. H. Bucksbaum, Population trapping in Kr and Xe in intense laser fields, Phys. Rev. A **47**, R49(R) (1993).

[41] B. Feuerstein, R. Moshammer, D. Fischer, A. Dorn, C. D. Schröter, J. Deipenwisch, J. R. Crespo Lopez-Urrutia, C. Höhr, P. Neumayer, J. Ullrich, H. Rottke, C. Trump, M. Wittmann, G. Korn, and W. Sandner, Separation of Recollision Mechanisms in Nonsequential Strong Field Double Ionization of Ar: The Role of Excitation Tunneling, Phys. Rev. Lett. **87**, 043003 (2001).

[42] A. Diaspro, P. Bianchini, G. Vicidomini, M. Faretta, P. Ramoino, and C. Usai, Multi-photon excitation microscopy, BioMed. Eng. OnLine **5**, 36 (2006).

[43] T. Streibel and R. Zimmermann, Resonance-enhanced multi-photon ionization mass spectrometry (REMPI-MS): Applications for process analysis, Annu. Rev. Anal. Chem. **7**, 361 (2014).

[44] T. Nubbemeyer, K. Gorling, A. Saenz, U. Eichmann, and W. Sandner, Strong-Field Tunneling Without Ionization, Phys. Rev. Lett. **101**, 233001 (2008).

[45] P. L. Knight, M. A. Lauder, and B. J. Dalton, Laser-induced continuum structure, Phys. Rep. **190**, 1 (1990).

[46] S. Chen, M. J. Bell, A. R. Beck, H. Mashiko, M. Wu, A. N. Pfeiffer, M. B. Gaarde, D. M. Neumark, S. R. Leone, and K. J. Schafer, Light-induced states in attosecond transient absorption spectra of laser-dressed helium, Phys. Rev. A **86**, 063408 (2012).

[47] F. He, C. Ruiz, A. Becker, and U. Thumm, Attosecond probing of instantaneous ac Stark shifts in helium atoms, J. Phys. B **44**, 211001 (2011).

[48] M. Chini, B. Zhao, H. Wang, Y. Cheng, S. X. Hu, and Z. Chang, Subcycle ac Stark Shift of Helium Excited States Probed with Isolated Attosecond Pulses, Phys. Rev. Lett. **109**, 073601 (2012).

[49] U. Eichmann, A. Saenz, S. Eilzer, T. Nubbemeyer, and W. Sandner, Observing Rydberg Atoms to Survive Intense Laser Fields, Phys. Rev. Lett. **110**, 203002 (2013).

[50] M. Gavrila, Atomic stabilization in superintense laser fields, J. Phys. B **35**, R147 (2002).

[51] L. Fechner, N. Camus, J. Ullrich, T. Pfeifer, and R. Moshammer, Strong-Field Tunneling from a Coherent Superposition of Electronic States, Phys. Rev. Lett. **112**, 213001 (2014).

[52] L. Fechner, N. Camus, A. Krupp, J. Ullrich, T. Pfeifer, and R. Moshammer, Creation and survival of autoionizing states in strong laser fields, Phys. Rev. A **92**, 051403(R) (2015).

[53] M. Th. Hassan, T. T. Luu, A. Moulet, O. Raskazovskaya, P. Zhokhov, M. Garg, N. Karpowicz, A. M. Zheltikov, V. Pervak, F. Krausz, and E. Goulielmakis, Optical attosecond pulses and tracking the nonlinear response of bound electrons, Nature (London) **530**, 66 (2016).

[54] H. Zimmermann, S. Patchkovskii, M. Ivanov, and U. Eichmann, Unified Time and Frequency Picture of Ultrafast Atomic Excitation in Strong Laser Fields, Phys. Rev. Lett. **118**, 013003 (2017).

[55] H. Yun, J. H. Mun, S. I. Hwang, S. B. Park, I. A. Ivanov, C. H. Nam, and K. T. Kim, Coherent extreme-ultraviolet emission generated through frustrated tunnelling ionization, Nat. Photon. **12**, 620 (2018).

[56] W.-C. Jiang, X.-M. Tong, R. Pazourek, S. Nagele, and J. Burgdörfer, Theory of bound-state coherences generated and probed by optical attosecond pulses, Phys. Rev. A **101**, 053435 (2020).

[57] A. C. Bray, A. S. Maxwell, Y. Kissin, M. Ruberti, M. F. Ciappina, V. Averbukh, and C. F. de Morisson Faria, Polarization in strong-field ionization of excited helium, J. Phys. B **54**, 194002 (2021).

[58] D. J. Tannor, *Introduction to Quantum Mechanics: A Time-Dependent Perspective* (University Science Books, Sausalito, 2007).

[59] D. B. Milošević, G. G. Paulus, D. Bauer, and W. Becker, Above-threshold ionization by few-cycle pulses, J. Phys. B **39**, R203 (2006).

[60] B. Fetić, W. Becker, and D. B. Milošević, Extracting photoelectron spectra from the time-dependent wave function: Comparison of the projection onto continuum states and window-operator methods, Phys. Rev. A **102**, 023101 (2020).

[61] W. Becker, and D. B. Milošević, A gauge-covariant derivation of the strong-field approximation, Laser Phys. **19**, 1621 (2009).

[62] A. Esquembre Kučukalić, W. Becker, and D. B. Milošević, Application of the phase-space path integral to strong-laser-field-assisted electron-ion radiative recombination: A gauge-covariant formulation, Symmetry **12**, 1606 (2020).

[63] C. F. de Morisson Faria and A. S. Maxwell, It is all about phases: Ultrafast holographic photoelectron imaging, Rep. Prog. Phys. **83**, 034401 (2020).

[64] M. Kübel, P. Wustelt, Y. Zhang, S. Skruszewicz, D. Hoff, D. Würzler, H. Kang, D. Zille, D. Adolph, G. G. Paulus, A. M. Sayler, M. Dumergue, A. Nayak, R. Flender, L. Haizer, M. Kurucz, B. Kiss, S. Kühn, B. Fetić, and D. B. Milošević, High-Order Phase-Dependent Asymmetry in the Above-Threshold Ionization Plateau, Phys. Rev. Lett. **126**, 113201 (2021).

[65] D. B. Milošević, in *Ultrafast Dynamics Driven by Intense Light Pulses*, edited by M. Kitzler and S. Gräfe (Springer, Switzerland, 2016), Chap. 2, pp. 27–47.

[66] R. N. Hill, in *Handbook of Atomic, Molecular, and Optical Physics*, edited by G. W. F. Drake (Springer Science+Business Media, New York, 2006), Chap. 9, pp. 153–171.

[67] I. S. Gradshteyn and I. M. Ryzhik, *Tables of Integrals, Series, and Products*, 5th ed. (Academic, New York, 1994), Chap. 8.93.

[68] L. F. DiMauro and P. Agostini, Ionization dynamics in strong laser fields, Adv. At. Mol. Opt. Phys. **35**, 79 (1995).

[69] A. Kramida, Y. Ralchenko, *J. Reader, and NIST ASD Team, NIST Atomic Spectra Database*, https://physics.nist.gov/asd (National Institute of Standards and Technology, Gaithersburg, 2020).